applied sciences

MDPI

Article

Design and Validation of the Invariant Imbedded T-Matrix Scattering Model for Atmospheric Particles with Arbitrary Shapes

Shuai Hu [1,2], Lei Liu [1,*], Taichang Gao [2] and Qingwei Zeng [1]

[1] College of Meteorology and Oceanography, National University of Defense Technology, Nanjing 211101, China; hushuai2012@hotmail.com (S.H.); zengqingwei519@yahoo.com (Q.Z.)

[2] National Key Laboratory on Electromagnetic Environment and Electro-Optical Engineering, National University of Defense Technology, Nanjing 211101, China; 2009gaotc@gmail.com

* Correspondence: liuleidll@gmail.com

Received: 4 September 2019; Accepted: 15 October 2019; Published: 18 October 2019

Abstract: Light scattering by non-spherical particles is an important factor influencing atmospheric radiative transfer. To accurately simulate the scattering properties of non-spherical particles, the Invariant Imbedded T-matrix method (IIM T-Matrix) is developed by combining the Lorenz–Mie theory and invariant imbedding technique. In this model, the non-spherical particle is regarded as an inhomogeneous sphere and discretized into multiple spherical layers in the spherical coordinate system. The T-matrix of the inscribed sphere is firstly calculated by the Lorenz–Mie theory, and then taking it as the initial value, the T-matrix is updated layer by layer by using the invariant imbedding technique. To improve the computational efficiency, the model is further parallelized by the OpenMP technique. To verify the simulation accuracy of the IIM T-Matrix method, the results of the model are compared with those of the EBCM (Extended Boundary Condition Method) T-Matrix method, DDA (Discrete Dipole Approximation) and MRTD (Multi-Resolution Time Domain). The results show that the scattering phase matrix simulated by the IIM T-Matrix method closely agrees with that of the well-tested models, indicating that the IIM T-Matrix method is a powerful tool for the light scattering simulation of non-spherical particles. Since the IIM T-Matrix method is derived from the volume integral equation, compared to the T-Matrix method which is based on surface integral principles (i.e., "EBCM" or the "null field method"), it can be applied to the scattering calculations of particle with arbitrary shapes and inhomogeneous compositions, which can greatly expand the application scope of the T-Matrix method.

Keywords: light scattering; non-spherical particles; invariant imbedding T-Matrix method; Lorenz–Mie theory; non-rotationally symmetric particle

1. Introduction

The light scattering and absorption by non-spherical particles (such as ice crystals, dust aerosols, etc.) plays an important role in the atmospheric radiative transfer [1–4]. However, because of the irregular shape of these particles, there is still considerable uncertainty in their scattering characteristics [5–7], which has become an important factor restricting the accuracy of atmospheric remote sensing [8,9]. For polarized remote sensing, the effect of the "non-spherical effect" is much more remarkable since the polarization of diffuse light is very sensitive to the particles' shape [10,11]. Therefore, how to obtain the scattering properties of these non-spherical particles accurately has become a hot issue in the field of atmospheric radiation [9,12–14].

In order to simulate the light scattering by non-spherical particles, many scattering computational models were established [15,16]. Typical models include the T-matrix method [17,18], Discrete Dipole

Approximation (DDA) [19,20], Finite Difference Time Domain (FDTD) [21,22], Pseudo-Spectral Time Domain (PSTD) [23–25], and Multi-Resolution Time Domain (MRTD) [26,27]. DDA and FDTD can be applied to the light scattering calculation for particles with arbitrary shape; however, due to the limitation of their computational stability and complexity, it is a tough job for them to simulate the light scattering by particles with large sizes [15]. Although PSTD and MRTD can calculate the scattering properties of large particles, their scattering simulation processes are closely related to particle's orientation and incident light (propagation direction and polarization state). Namely, as long as any of these parameters changes, their scattering processes need to be re-simulated as well [15,16]. Therefore, if the scattering properties of the particles with certain orientation distributions are needed to be calculated, the computational process should be repeated many times, which will be very time-consuming (DDA and FDTD also have the same problem). In contrast, the T-matrix method has a significant advantage over these models. Since the T-matrix is a complete dataset of scattering information which only depends on the refractive index, size, and shape of the particle, the scattering properties for arbitrary orientations can be calculated analytically once the T-matrix is obtained [28]. In the traditional T-matrix models, the T-matrix is calculated by the Extended Boundary Condition Method (EBCM, also known as the "null-field method") [29,30]. Though these models are very efficient at calculating light scattering by particles with ideal morphologies, like spheres, spheroids, and cylinders [18,31,32], they generally have limited applicability to the irregularly shaped aerosol and ice crystal particles [15]. Besides, with the increase of particle size and refractive index, their calculation processes will become divergent. In the actual applications, many researchers have also found that the performance is highly doubtful if the non-spherical aerosol particles are taken as the spherical or spheroidal ones in a radiative transfer simulation [9,33]. Considering the tremendous advantage of the T-matrix, many scholars have attempted to calculate the T-matrix by other methods, except the EBCM. For example, Schulz used the Separation of Variable Method (SVM) to calculate the T-matrix of spheroidal particles [34]. Mackowski et al. applied the Discrete Dipole Approximation to calculate the T-matrix of the non-spherical particles [35], while Loke et al. [36] tried to combine the DDA with the Point Matching Method (PMM) to calculate the T-matrix. However, similar to the DDA, most of these methods can only be applied to simulate the light scattering by small particles.

In order to obtain the T-matrix of the particles with irregular shapes, Yang and Bi also applied the Invariant Imbedding (IIM) T-Matrix method to the light scattering calculation [31,37,38]. The IIM T-Matrix model was first proposed by Johnson [39], but due to the limitation of computing ability at that time, it has not attracted enough attention. With the development of computer technology, Bi rewrote the T-matrix model by combining the invariant embedding technique with the separation of variables method (SOV) and the EBCM method. Now, by using this model, not only can the light scattering by particles with arbitrary shapes and large sizes be effectively simulated, but also, the computations can be performed with a high efficiency. In this paper, we also developed an invariant embedding T-matrix model independently, in which the T-matrix is calculated by combining the invariant embedding technique with the Lorenz–Mie theory.

This paper is organized as follows: firstly, the concept of T-matrix is briefly introduced, then, the basic principle and implementation of the IIM T-Matrix method is given. Next, an acceleration scheme is proposed by combining the Lorenz–Mie theory and the invariant imbedding technique. In Section 3, the simulation accuracy of the IIM T-Matrix method is validated against the well-tested scattering models. In Section 4, the modeling efficiency of the IIM T-Matrix code is discussed. Section 5 is a brief summary of this paper.

2. The Principle of the Invariant Imbedding (IIM) T-Matrix Method

In this Section, the principle of the Invariant Imbedding T-matrix method is introduced in the following way: firstly, the T-matrix is introduced, then, the basic equations to calculate the T-matrix are derived from the Helmholtz Volume Integral Equation in Section 2.2. To simplify the calculation equation of the T-matrix, the invariant imbedding technique to calculate the T-matrix is briefly

introduced in Section 2.3. Further, the acceleration scheme based on the Lorenz–Mie theory is proposed in Section 2.4.

2.1. A Brief Introduction of the T-Matrix

The T-matrix is a linear transformation matrix of the expansion coefficients of incident and scattered fields. In order to obtain the T-matrix, the incident and scattered fields should first be expanded by vector spherical harmonic functions [16,29], shown as:

$$\mathbf{E}_{inc}(\mathbf{r}) = \sum_{n=1}^{\infty}\sum_{m=-n}^{n} a_{mn} Rg\mathbf{M}_{mn}(kr,\theta,\varphi) + b_{mn} Rg\mathbf{N}_{mn}(kr,\theta,\varphi) \tag{1}$$

$$\mathbf{E}_{sca}(\mathbf{r}) = \sum_{n=1}^{\infty}\sum_{m=-n}^{n} p_{mn}\mathbf{M}_{mn}(kr,\theta,\varphi) + q_{mn}\mathbf{N}_{mn}(kr,\theta,\varphi),\ (r > R) \tag{2}$$

where, R is the radius of the smallest circumscribed sphere of the scatterer centered at the origin of the laboratory coordinate system. $Rg\mathbf{M}_{mn}(kr,\theta,\varphi)$ and $Rg\mathbf{N}_{mn}(kr,\theta,\varphi)$ are the regular vector spherical wave functions, $\mathbf{M}_{mn}(kr,\theta,\varphi)$ and $\mathbf{N}_{mn}(kr,\theta,\varphi)$ are the vector spherical wave functions,p_{mn} and q_{mn} are the expansion coefficients of the scattering electric field, and a_{mn} and b_{mn} are the expansion coefficients of the incident field. The definition of the vector spherical wave functions can be found in the Appendix A of this paper.

Since the Maxwell equations are linear, the expansion coefficients of incident light (a_{mn} and b_{mn}) and scattered light (p_{mn} and q_{mn}) can also be converted by a linear transformation. The linear transformation matrix is just the T-matrix, which can be expressed as:

$$p_{mn} = \sum_{n'=1}^{\infty}\sum_{m'=-n'}^{n'}\left[T^{11}_{mnm'n'}a_{m'n'} + T^{12}_{mnm'n'}b_{m'n'}\right] \tag{3}$$

$$q_{mn} = \sum_{n'=1}^{\infty}\sum_{m'=-n'}^{n'}\left[T^{21}_{mnm'n'}a_{m'n'} + T^{22}_{mnm'n'}b_{m'n'}\right] \tag{4}$$

In order to express the T-matrix more intuitively and compactly, the two formulas above can be written into matrix form, given as:

$$\begin{bmatrix} p_1 \\ q_1 \\ \cdots \\ \cdots \\ p_{l_{\max}} \\ q_{l_{\max}} \end{bmatrix} = \mathbf{T}\begin{bmatrix} a_1 \\ b_1 \\ \cdots \\ \cdots \\ a_{l_{\max}} \\ b_{l_{\max}} \end{bmatrix} = \begin{bmatrix} T^{11}_{11} & T^{12}_{11} & \cdots & \cdots & T^{11}_{1l_{\max}} & T^{12}_{1l_{\max}} \\ T^{21}_{11} & T^{22}_{11} & \cdots & \cdots & T^{21}_{1l_{\max}} & T^{22}_{1l_{\max}} \\ \cdots & \cdots & \cdots & \cdots & \cdots & \cdots \\ \cdots & \cdots & \cdots & \cdots & \cdots & \cdots \\ T^{11}_{l_{\max}1} & T^{12}_{l_{\max}1} & \cdots & \cdots & T^{11}_{l_{\max}l_{\max}} & T^{12}_{l_{\max}l_{\max}} \\ T^{21}_{l_{\max}1} & T^{22}_{l_{\max}1} & \cdots & \cdots & T^{21}_{l_{\max}l_{\max}} & T^{22}_{l_{\max}l_{\max}} \end{bmatrix}\begin{bmatrix} a_1 \\ b_1 \\ \cdots \\ \cdots \\ a_{l_{\max}} \\ b_{l_{\max}} \end{bmatrix} \tag{5}$$

in which, the T-matrix is a $2l_{max} \times 2l_{max}$ super-matrix, where, $l_{max} = n_{max}(n_{max}+2)$ (n_{max} is the highest expansion order of the field components).

2.2. Discretization and Vectorization of the Helmholtz Volume Integral Equation

The physical basis of the IIM T-matrix method is the Helmholtz volume integral equation. If we take the time dependence of the electromagnetic wave as $\exp(-j\omega t)$, then the equation in frequency domain can be expressed as [40]:

$$\mathbf{E}(\mathbf{r}) = \mathbf{E}_{inc}(\mathbf{r}) + \iiint_V \mathbf{G}_0(\mathbf{r},\mathbf{r}')u(\mathbf{r}')\mathbf{Z}(\mathbf{r})\mathbf{E}(\mathbf{r}')d^3\mathbf{r}' \tag{6}$$

in which, $\mathbf{E}$ denotes the electric vector, $u(\mathbf{r}) = k^2(\varepsilon_r(\mathbf{r}) - 1)$, k is the wavenumber, $\mathbf{r}$ is the position vector,$\varepsilon_r(\mathbf{r})$ is the relative permittivity of the medium, $\mathbf{E}_{inc}(\mathbf{r})$ is the electric vector of incident wave, $\mathbf{G}_0(\mathbf{r}, \mathbf{r}')$ denotes the free space dyadic Green's function, and $\mathbf{Z}(\mathbf{r})$ is a transformation matrix determined by the particle's permittivity, the expressions of $\mathbf{G}_0(\mathbf{r}, \mathbf{r}')$ and $\mathbf{Z}(\mathbf{r})$ are shown in Equations (7) and (8).

$$\mathbf{G}_0(\mathbf{r}, \mathbf{r}') = (\mathbf{I} + \frac{1}{k^2}\nabla \otimes \nabla)\frac{\exp(ik|\mathbf{r} - \mathbf{r}'|)}{4\pi|\mathbf{r} - \mathbf{r}'|} \tag{7}$$

$$\mathbf{Z}(\mathbf{r}) = \frac{1}{\varepsilon_r(\mathbf{r})}\hat{\mathbf{r}} \otimes \hat{\mathbf{r}} + \hat{\boldsymbol{\theta}} \otimes \hat{\boldsymbol{\theta}} + \hat{\boldsymbol{\varphi}} \otimes \hat{\boldsymbol{\varphi}} \tag{8}$$

In the equations above, the operator "⊗" denotes the dyad product, i.e., if $\mathbf{a}$ and $\mathbf{b}$ are two column vectors, then $\mathbf{a} \otimes \mathbf{b} = \mathbf{a} \cdot \mathbf{b}^T$.

In order to realize the discretization of Equation (6), both field components and dyadic Green's function $\mathbf{G}_0(\mathbf{r}, \mathbf{r}')$ need to be expanded by vector spherical harmonic functions. Therefore, the expansion and vectorization of the field components and dyad Green's function are firstly introduced, and then the discretization scheme of volume integral equation is further derived.

a. Expansion and vectorization of the field components and dyad Green's function $\mathbf{G}_0(\mathbf{r}, \mathbf{r}')$. The expansion expression of the incident field has been given by Equation (1), which can be written into matrix form, given as:

$$\mathbf{E}_{inc}(\mathbf{r}) = \sum_{n=1}^{\infty}\sum_{m=-n}^{n}(Rg\mathbf{M}_{mn}, Rg\mathbf{N}_{mn})\begin{pmatrix} a_{mn} \\ b_{mn} \end{pmatrix} = \sum_{n=1}^{\infty}\sum_{m=-n}^{n}\overline{\overline{\mathbf{Y}}}_{mn}(\theta, \varphi)\bar{\bar{\mathbf{J}}}_n(kr)\begin{pmatrix} a_{mn} \\ b_{mn} \end{pmatrix} \tag{9}$$

where, $\overline{\overline{\mathbf{Y}}}_{mn}(\theta, \varphi)$ is an angular function matrix, and $\bar{\bar{\mathbf{J}}}_n(kr)$ is the radial Bessel function matrix, which can be written as:

$$\overline{\overline{\mathbf{Y}}}_{mn}(\theta, \varphi) = (-1)^m \exp(im\varphi)\left[\frac{2n+1}{4\pi n(n+1)}\right]^{1/2} \cdot \begin{pmatrix} 0 & 0 & \sqrt{n(n+1)}d^n_{0m}(\theta) \\ i\pi_{mn}(\theta) & \tau_{mn}(\theta) & 0 \\ \tau_{mn}(\theta) & i\pi_{mn}(\theta) & 0 \end{pmatrix}, \bar{\bar{\mathbf{J}}}_n(kr) = \begin{pmatrix} J_n(kr) & 0 \\ 0 & \frac{1}{kr}\frac{d}{d(kr)}(krJ_n(kr)) \\ 0 & \frac{\sqrt{n(n+1)}}{kr}J_n(kr) \end{pmatrix}$$

where, $d^n_{0m}(\theta)$ is the Wigner-d function, while $\pi_{mn}(\theta)$ and $\tau_{mn}(\theta)$ are the angular functions, given by:

$$\pi_{mn}(\theta) = \frac{m}{\sin\theta}d^n_{0m}(\theta);\ \tau_{mn}(\theta) = \frac{d}{d\theta}d^n_{0m}(\theta) \tag{10}$$

Similarly, the total field can also be expanded by the vector spherical harmonic functions and written into matrix form, expressed as:

$$\mathbf{E}(\mathbf{r}) = \sum_{n=1}^{\infty}\sum_{m=-n}^{n}(\mathbf{M}_{mn}, \mathbf{N}_{mn})\mathbf{E}_{mn} = \sum_{n=1}^{\infty}\sum_{m=-n}^{n}\overline{\overline{\mathbf{Y}}}_{mn}(\theta, \varphi)\overline{\overline{\mathbf{H}}}_n(kr)\mathbf{E}_{mn} \tag{11}$$

where, $\mathbf{E}_{mn}$ is the expansion coefficients of the total field, and $\overline{\overline{\mathbf{H}}}_n(kr)$ is the radial Hankel function matrix, whose form is similar to $\bar{\bar{\mathbf{J}}}_n(kr)$, expressed as:

$$\overline{\overline{\mathbf{H}}}_n(kr) = \begin{pmatrix} H^{(1)}_n(kr) & 0 \\ 0 & \frac{1}{kr}\frac{d}{d(kr)}\left(krH^{(1)}_n(kr)\right) \\ 0 & \frac{\sqrt{n(n+1)}}{kr}H^{(1)}_n(kr) \end{pmatrix} \tag{12}$$

Similar to the field components, the dyadic Green's function $\mathbf{G}_0(\mathbf{r},\mathbf{r}')$ should also be expanded by the vector spherical harmonic functions, but in the case that $r > r'$ and $r < r'$, their expansion forms are slightly different, written as:

$$\overline{\overline{\mathbf{G}}}_0(\mathbf{r},\mathbf{r}') = \begin{cases} ik\sum\limits_{n=1}^{\infty}\sum\limits_{m=-n}^{n} & (-1)^m\mathbf{M}_{-mn}(kr,\theta,\varphi)\otimes Rg\mathbf{M}_{mn}(kr',\theta',\varphi') \\ & +(-1)^m\mathbf{N}_{-mn}(kr,\theta,\varphi)\otimes Rg\mathbf{N}_{mn}(kr',\theta',\varphi')\ r > r' \\ ik\sum\limits_{n=1}^{\infty}\sum\limits_{m=-n}^{n} & (-1)^m Rg\mathbf{M}_{-mn}(kr,\theta,\varphi)\otimes\mathbf{M}_{mn}(kr',\theta',\varphi') \\ & +(-1)^m Rg\mathbf{N}_{-mn}(kr,\theta,\varphi)\otimes\mathbf{N}_{mn}(kr',\theta',\varphi')\ r < r' \end{cases} \tag{13}$$

Because the expansion of the dyadic Green's function is similar for $r > r'$ and $r < r'$ on the whole, here we only introduce the matrix expansion process of $\mathbf{G}_0(\mathbf{r},\mathbf{r}')$ for $r > r'$. From the symmetry of the dyadic Green's function, the following equation can be easily derived, given as:

$$\overline{\overline{\mathbf{G}}}_0(\mathbf{r},\mathbf{r}') = ik\sum_{n=1}^{\infty}\sum_{m=-n}^{n} \begin{matrix} (-1)^m\mathbf{M}_{mn}(kr,\theta,\varphi)\otimes Rg\mathbf{M}_{-mn}(kr',\theta',\varphi') \\ +(-1)^m\mathbf{N}_{mn}(kr,\theta,\varphi)\otimes Rg\mathbf{N}_{-mn}(kr',\theta',\varphi') \end{matrix} \tag{14}$$

By using the symmetric relations of the vector spherical harmonic function [16], Equation (13) can be simplified and rewritten it into the matrix form, expressed as:

$$\overline{\overline{\mathbf{G}}}_0(\mathbf{r},\mathbf{r}') = \overline{\overline{\mathbf{Y}}}_{mn}(\theta,\varphi)\overline{\overline{g}}_n(r,r')\left(\overline{\overline{\mathbf{Y}}}^*_{mn}(\theta',\varphi')\right)^T \tag{15}$$

where, $\overline{\overline{g}}_n(r,r')$ is a matrix constructed by the Bessel and Hankel functions, written as:

$$\overline{\overline{g}}_n(r,r') = ik\overline{\overline{\mathbf{H}}}_n(kr)\overline{\overline{\mathbf{J}}}^T_n(kr') \tag{16}$$

Similarly, for $r < r'$, the dyad Green's function $\overline{\overline{\mathbf{G}}}_0(\mathbf{r},\mathbf{r}')$ can also be written into the matrix form, similar to Equation (15), written as:

$$\begin{aligned} \overline{\overline{\mathbf{G}}}_0(\mathbf{r},\mathbf{r}') &= ik\overline{\overline{\mathbf{Y}}}_{mn}(\theta,\varphi)\overline{\overline{\mathbf{H}}}_n(kr)\overline{\overline{\mathbf{J}}}^T_n(kr')\left(\overline{\overline{\mathbf{Y}}}^*_{mn}(\theta',\varphi')\right)^T \\ &= \overline{\overline{\mathbf{Y}}}_{mn}(\theta,\varphi)\overline{\overline{g}}_n(r,r')\left(\overline{\overline{\mathbf{Y}}}^*_{mn}(\theta',\varphi')\right)^T \end{aligned} \tag{17}$$

$$\overline{\overline{g}}_n(r,r') = ik\overline{\overline{\mathbf{J}}}_n(kr)\overline{\overline{\mathbf{H}}}^T_n(kr') \tag{18}$$

On the condition that $r = r'$, the expansion coefficients of $\overline{\overline{\mathbf{G}}}_0(\mathbf{r},\mathbf{r}')$ are taken as the average value of those for $r > r'$ and $r < r'$. In this case, the matrix form of the dyad Green's function is similar to that of Equation (15), but the matrix $\overline{\overline{g}}_n(r,r')$ should be rewritten as:

$$\overline{\overline{g}}_n(r,r') = ik\left(\overline{\overline{\mathbf{J}}}_n(kr)\overline{\overline{\mathbf{H}}}_n(kr') + \overline{\overline{\mathbf{H}}}_n(kr)\overline{\overline{\mathbf{J}}}_n(kr')\right)/2 \tag{19}$$

b. The discretization of the volume integral equation. Substitute the expansion equations of the field components and the dyadic Green's function into Equation (6), and use the orthogonality of the vector spherical harmonic function for simplification, then, the following integral formulas can be obtained for each (m, n), written as:

$$\begin{aligned} &\mathbf{E}_{m'n'}(r,\theta,\varphi) = \overline{\overline{\mathbf{Y}}}_{m'n'}(\theta,\varphi)\overline{\overline{\mathbf{J}}}_{n'}(kr) \\ &+\int_V dr'r'^2d\Omega'\sum_{n=1}^{\infty}\sum_{m=-n}^{n}\overline{\overline{\mathbf{Y}}}_{mn}(\theta,\varphi)\overline{\overline{g}}_n(r,r')\left(\overline{\overline{\mathbf{Y}}}^*_{mn}(\theta',\varphi')\right)^T u(\mathbf{r}')\overline{\overline{\mathbf{Z}}}(\mathbf{r}')\mathbf{E}_{m'n'}(\mathbf{r}') \end{aligned} \tag{20}$$

For further simplification, we define the vector amplitude density function $\mathbf{F}_{mnm'n'}(r)$ as:

$$\mathbf{F}_{mnm'n'}(r) = \int_{\Omega} \left(\overline{\overline{\mathbf{Y}}}^{*}_{mn}(\theta,\varphi)\right)^{T} u(\mathbf{r})\overline{\overline{\mathbf{Z}}}(\mathbf{r})\mathbf{E}_{m'n'}(\mathbf{r})d\Omega \tag{21}$$

This parameter is related to the electric current density and can be thought of as the source of the scattered electric wave. Then, by substituting the equation above into Equation (20), we can get:

$$\mathbf{E}_{m'n'}(r,\theta,\varphi) = \overline{\overline{\mathbf{Y}}}_{m'n'}(\theta,\varphi)\overline{\overline{\mathbf{J}}}_{n'}(kr) + \int_{0}^{R} dr' \sum_{n=1}^{\infty}\sum_{m=-n}^{n} \overline{\overline{\mathbf{Y}}}_{mn}(\theta,\varphi)\overline{\overline{g}}_{n}(r,r')\mathbf{F}_{mnm'n'}(r') \tag{22}$$

Further, we insert Equation (22) into Equation (21), then the following relation can be obtained after some simplification, given as:

$$\mathbf{F}_{mnm'n'}(r) = \overline{\overline{\mathbf{U}}}_{mnm'n'}(r)\overline{\overline{\mathbf{J}}}_{n'}(kr) + \int_{0}^{R} dr' \sum_{\widetilde{n}=1}^{\infty}\sum_{\widetilde{m}=-\widetilde{n}}^{\widetilde{n}} \overline{\overline{\mathbf{U}}}_{mnm'n'}(r)\overline{\overline{g}}_{\widetilde{n}}(r,r')\mathbf{F}_{\widetilde{m}\widetilde{n}m'n'}(r') \tag{23}$$

where, $\overline{\overline{\mathbf{U}}}_{mnm'n'}(r)$ is the surface integral matrix of the spherical shell, written as:

$$\overline{\overline{\mathbf{U}}}_{mnm'n'}(r) = r^2 \int_{\Omega} d\Omega' \left(\overline{\overline{\mathbf{Y}}}^{*}_{mn}(\theta',\varphi')\right)^{T} u(\mathbf{r}')\overline{\overline{\mathbf{Z}}}(\mathbf{r}')\overline{\overline{\mathbf{Y}}}_{m'n'}(\theta,\varphi) \tag{24}$$

From the formula above, we can find that the U-matrix contains the spatial distribution information of the scatterer, that is, the irregular shape of particles and its material distribution can be manifested by this matrix, so its calculation accuracy is very important in the IIM T-Matrix model.

Since the scattering field usually refers to the electromagnetic field at infinite distance, in this case, matrix $\overline{\overline{g}}_{n}$ has the form of $\overline{\overline{g}}_{n}(r,r') = ik\overline{\overline{\mathbf{H}}}(kr)\overline{\overline{\mathbf{J}}}^{T}_{nn}(kr')$, since r is larger than r' in the far field. Then, substitute matrix $\overline{\overline{g}}_{n}$ into Equation (26), and we can obtain:

$$\mathbf{E}_{m'n'}(r,\theta,\varphi) = \overline{\overline{\mathbf{Y}}}_{m'n'}(\theta,\varphi)\overline{\overline{\mathbf{J}}}_{n'}(kr) + \int_{0}^{R} dr' \sum_{n=1}^{\infty}\sum_{m=-n}^{n} \overline{\overline{\mathbf{Y}}}_{mn}(\theta,\varphi)\overline{\overline{\mathbf{H}}}_{n}(kr)\overline{\overline{\mathbf{T}}}_{mnm'n'} \tag{25}$$

where, $\overline{\overline{\mathbf{T}}}_{mnm'n'}$ is the T-matrix introduced in Section 2.1, which can be calculated by:

$$\overline{\overline{\mathbf{T}}}_{mnm'n'} = ik\int_{0}^{R} \overline{\overline{\mathbf{J}}}^{T}_{n}(kr')\overline{\overline{\mathbf{F}}}_{mnm'n'}(r')dr' \tag{26}$$

Equations (23), (25), and (26) constitute the basic equation set for the calculation of the T-matrix. By solving these equations, the T-matrix can be obtained directly, and the scattering parameters can also be calculated based on the T-matrix elements.

In order to solve the equations above, the radial integrals in Equations (25) and (26) should be discretized by Gaussian quadrature, which yields:

$$\begin{aligned}\overline{\overline{\mathbf{F}}}_{mnm'n'}(r_i) = {} & \overline{\overline{\mathbf{U}}}_{mnm'n'}(r_i)\overline{\overline{\mathbf{J}}}_{n'}(kr_i) \\ & + \sum_{j=1}^{N} \omega_j \sum_{\widetilde{n}=1}^{\infty}\sum_{\widetilde{m}=-\widetilde{n}}^{\widetilde{n}} \overline{\overline{\mathbf{U}}}_{mnm'n'}(r_i)\overline{\overline{g}}_{\widetilde{n}}(r_i,r_j)\mathbf{F}_{\widetilde{m}\widetilde{n}m'n'}(r_j)\end{aligned} \tag{27}$$

$$\overline{\overline{\mathbf{T}}}_{mnm'n'} = ik\sum_{j=1}^{N} \omega_j \overline{\overline{\mathbf{J}}}_n^T(kr_j)\overline{\overline{\mathbf{F}}}_{mnm'n'}(r_j) \tag{28}$$

where, $r_j (j = 1, 2 \ldots, N)$ are the Gaussian quadrature points, and ω_j is the weight factor for each Gaussian point. Further, the above two formulas can be written into the matrix form, expressed as:

$$\overline{\overline{\mathbf{F}}}(r_i) = \overline{\overline{\mathbf{U}}}(r_i)\overline{\overline{\mathbf{J}}}(kr_i) + \sum_{j=1}^{N} \omega_j \overline{\overline{\mathbf{U}}}(r_i)\overline{\overline{\mathbf{g}}}(r_i, r_j)\overline{\overline{\mathbf{F}}}(r_j) \tag{29}$$

$$\overline{\overline{\mathbf{T}}} = ik\sum_{j=1}^{N} \omega_j \overline{\overline{\mathbf{J}}}^T(kr_j)\overline{\overline{\mathbf{F}}}(r_j) \tag{30}$$

where, $\overline{\overline{\mathbf{J}}}(kr_i)$ and $\overline{\overline{\mathbf{g}}}(r_i, r_j)$ are the super-matrices with $\overline{\overline{\mathbf{J}}}_{n'}(kr_i)$ and $\overline{\overline{g}}_n(r, r')$ as the element, and $\overline{\overline{\mathbf{F}}}(r_i)$ and $\overline{\overline{\mathbf{U}}}(r_i)$ are the super-matrices comprised by $\overline{\overline{\mathbf{F}}}_{mnm'n'}$ and $\overline{\overline{\mathbf{U}}}_{mnm'n'}$. The expression of $\overline{\overline{\mathbf{T}}}$ matrix is shown in Equation (5).

2.3. T-Matrix Computation Based on the Invariant Embedding Technique

In principle, Equation (29) is essentially a linear equation system, and can be solved by standard numerical methods, such as the Gaussian elimination method, the conjugate gradient method, etc., after $\overline{\overline{\mathbf{F}}}(r_i)$ is obtained, and then, the T-matrix can be obtained easily by substituting $\overline{\overline{\mathbf{F}}}(r_i)$ into Equation (30). However, because the matrices involved in this model are all super-matrices, the implementation of this scheme is very difficult, especially for large particles. Therefore, in order to improve the computational efficiency of the T-matrix, Johnson [33] first introduced the invariant embedding technique into the light scattering simulation (this technique was originally developed to solve quantum mechanical scattering problems). This method not only has the advantage of high computational efficiency, but can also calculate the T-matrix directly without calculating the matrix $\overline{\overline{\mathbf{F}}}(r_i)$, so it can greatly reduce computational time and memory consumption.

According to Equations (29) and (30), the non-spherical particle should be discretized along the radial direction, which is equivalent to dividing the particle into multiple inhomogeneous spherical layers in the spherical coordinate system, as shown in Figure 1. In this way, the non-spherical particle can be viewed as an inhomogeneous sphere, i.e., a portion of the sphere has the dielectric properties of the scattering particle and the rest is regarded as a vacuum.

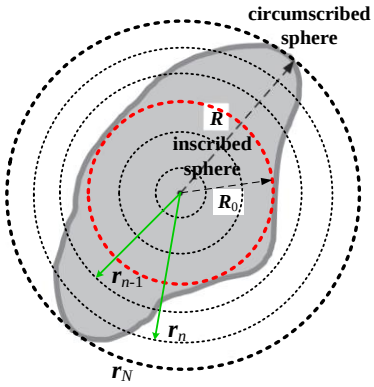

Figure 1. The discretization of the non-spherical particle in the spherical coordinate system.

Assuming n is an integer in $(1, N)$ (N is the number of the Gaussian integral points), then according to Equations (29) and (30), we define the matrix function $\mathbf{F}(n|r_i)$ and $\overline{\overline{\mathbf{T}}}(r_n)$, which satisfies the following equations:

$$\overline{\overline{\mathbf{F}}}(n|r_i) = \overline{\overline{\mathbf{U}}}(r_i)\overline{\overline{\mathbf{J}}}(r_i) + \sum_{j=1}^{n} \omega_j \overline{\overline{\mathbf{U}}}(r_i)\overline{\overline{\mathbf{g}}}(r_i, r_j)\overline{\overline{\mathbf{F}}}(n|r_j) \tag{31}$$

$$\overline{\overline{\mathbf{T}}}(r_n) = ik\sum_{j=1}^{n} \omega_j \overline{\overline{\mathbf{J}}}^{T}(r_j)\overline{\overline{\mathbf{F}}}(n|r_j) \tag{32}$$

where, $\overline{\overline{\mathbf{F}}}(n|r_i)$ and $\overline{\overline{\mathbf{T}}}(r_n)$ can be visually regarded as the vector amplitude density function and T-matrix of the sphere with nth spherical shell. From the Equations (31) and (32), it can be found that except for the fact that N is replaced by n, these equations are identical to Equations (29) and (30). Therefore, if we let $N = n$, we can obtain $\overline{\overline{\mathbf{F}}}(r_i) = \overline{\overline{\mathbf{F}}}(N|r_i)$ and $\overline{\overline{\mathbf{T}}} = \overline{\overline{\mathbf{T}}}(r_N)$.

Then, separate the nth term in the summation of Equation (31), and define $\overline{\overline{\mathbf{Q}}}(r_n)$ and $\overline{\overline{\mathbf{q}}}$ as follows:

$$\overline{\overline{\mathbf{Q}}}(r_n) = \omega_n\left[\overline{\overline{\mathbf{I}}} - \omega_n\overline{\overline{\mathbf{U}}}(r_n)\overline{\overline{\mathbf{g}}}(r_n, r_n)\right]^{-1}\overline{\overline{\mathbf{U}}}(r_n) \tag{33}$$

$$\overline{\overline{\mathbf{q}}} = ik\sum_{j=1}^{n-1} \omega_j \overline{\overline{\mathbf{J}}}^{T}(r_n, r_j)\overline{\overline{\mathbf{F}}}(n|r_j) \tag{34}$$

Then, Equation (31) can be simplified as:

$$\overline{\overline{\mathbf{F}}}(n|r_n) = {\omega_n}^{-1}\overline{\overline{\mathbf{Q}}}(r_n)\left[\overline{\overline{\mathbf{J}}}(kr_n) + \overline{\overline{\mathbf{H}}}(kr_n)\overline{\overline{\mathbf{q}}}\right] \tag{35}$$

where, $\overline{\overline{\mathbf{H}}}(kr)$ is a diagonal super-matrix with its element defined by Equation (12), ω_n is the weight factor of the nth Gaussian point. Because r_n is larger than r_j in Equation (35), $\overline{\overline{\mathbf{g}}}_n(r, r')$ has the expression of $\overline{\overline{\mathbf{g}}}_n(r, r') = ik\overline{\overline{\mathbf{H}}}(kr)\overline{\overline{\mathbf{J}}}^{T}(kr')$.

Equation (32) can be reshaped in a similar way. The nth term in the summation is firstly separated, together with Equation (35), then it can be simplified as:

$$\overline{\overline{\mathbf{T}}}(r_n) = \overline{\overline{\mathbf{q}}} + \overline{\overline{\mathbf{Q}}}_{11}(r_n) + \overline{\overline{\mathbf{Q}}}_{12}(r_n)\overline{\overline{\mathbf{q}}} \tag{36}$$

where, matrix $\overline{\overline{\mathbf{Q}}}_{11}(r_n)$ and $\overline{\overline{\mathbf{Q}}}_{12}(r_n)$ are two auxiliary matrices, defined as:

$$\overline{\overline{\mathbf{Q}}}_{11}(r_n) = \overline{\overline{\mathbf{J}}}^{T}(r_n)\overline{\overline{\mathbf{Q}}}(r_n)\overline{\overline{\mathbf{J}}}(r_n) \tag{37}$$

$$\overline{\overline{\mathbf{Q}}}_{12}(r_n) = \overline{\overline{\mathbf{J}}}^{T}(r_n)\overline{\overline{\mathbf{Q}}}(r_n)\overline{\overline{\mathbf{H}}}(r_n) \tag{38}$$

From the equations above, the relationship between matrix $\overline{\overline{\mathbf{F}}}(n|r_n)$, $\overline{\overline{\mathbf{T}}}(r_n)$ and $\overline{\overline{\mathbf{q}}}$ is established. However, $\overline{\overline{\mathbf{q}}}$ is still a super-matrix, therefore, we should further try to eliminate the matrix $\overline{\overline{\mathbf{F}}}(n|r_n)$ and $\overline{\overline{\mathbf{q}}}$ to establish the iterative equation only containing the $\overline{\overline{\mathbf{T}}}(r_n)$ matrix. First, from Equation (32), we can know that:

$$\overline{\overline{\mathbf{T}}}(r_{n-1}) = ik\sum_{j=1}^{n-1} \omega_j \overline{\overline{\mathbf{J}}}^{T}(r_j)\overline{\overline{\mathbf{F}}}(n-1|r_j) \tag{39}$$

Assuming that $\overline{\overline{\mathbf{F}}}(n|r_j) = \overline{\overline{\mathbf{F}}}(n-1|r_j)(\overline{\overline{\mathbf{I}}} + \overline{\overline{\mathbf{p}}})$ ($\overline{\overline{\mathbf{p}}}$ is a matrix), then from Equation (34), it can rewritten as:

$$\overline{\overline{\mathbf{T}}}(r_{n-1})(\overline{\overline{\mathbf{I}}} + \overline{\overline{\mathbf{p}}}) = \overline{\overline{\mathbf{q}}} \tag{40}$$

At the same time, we insert $\overline{\overline{\mathbf{F}}}(n|r_j) = \overline{\overline{\mathbf{F}}}(n-1|r_j)(\overline{\overline{\mathbf{I}}} + \overline{\overline{\mathbf{p}}})$ and $\overline{\overline{\mathbf{g}}}_n(r_i, r_n) = ik\overline{\overline{\mathbf{J}}}(kr_i)\overline{\overline{\mathbf{H}}}^T(kr_n)$ $(r_i < r_n)$ into Equation (31), a simplified expression between $\overline{\overline{\mathbf{p}}}$ and $\overline{\overline{\mathbf{q}}}$ can be obtained, written as:

$$\overline{\overline{\mathbf{p}}} = \overline{\overline{\mathbf{Q}}}_{21}(r_n) + \overline{\overline{\mathbf{Q}}}_{22}(r_n)\overline{\overline{\mathbf{q}}} \tag{41}$$

where, $\overline{\overline{\mathbf{Q}}}_{21}(r_n)$ and $\overline{\overline{\mathbf{Q}}}_{22}(r_n)$ are another two auxiliary matrices, which are defined as follows:

$$\overline{\overline{\mathbf{Q}}}_{21}(r_n) = \overline{\overline{\mathbf{H}}}^T(r_n)\overline{\overline{\mathbf{Q}}}(r_n)\overline{\overline{\mathbf{J}}}(r_n) \tag{42}$$

$$\overline{\overline{\mathbf{Q}}}_{22}(r_n) = \overline{\overline{\mathbf{H}}}^T(r_n)\overline{\overline{\mathbf{Q}}}(r_n)\overline{\overline{\mathbf{H}}}(r_n) \tag{43}$$

Then, by inserting Equation (41) into Equation (40), we can obtain:

$$\overline{\overline{\mathbf{T}}}(r_{n-1})(\overline{\overline{\mathbf{I}}} + \overline{\overline{\mathbf{Q}}}_{21}(r_n) + \overline{\overline{\mathbf{Q}}}_{22}(r_n)\overline{\overline{\mathbf{q}}}) = \overline{\overline{\mathbf{q}}} \tag{44}$$

The equation above can be regarded as a linear matrix equation of $\overline{\overline{\mathbf{q}}}$, through which the matrix $\overline{\overline{\mathbf{q}}}$ can be solved, written as:

$$\overline{\overline{\mathbf{q}}} = \left[\overline{\overline{\mathbf{I}}} - \overline{\overline{\mathbf{T}}}(r_{n-1})\overline{\overline{\mathbf{Q}}}_{22}(r_n)\right]\overline{\overline{\mathbf{T}}}(r_{n-1})\left[\overline{\overline{\mathbf{I}}} + \overline{\overline{\mathbf{Q}}}_{21}(r_n)\right] \tag{45}$$

At last, by substituting Equation (45) into Equation (36), the invariant imbedding iterative equation for the T-matrix can be obtained, given as:

$$\overline{\overline{\mathbf{T}}}(r_n) = \overline{\overline{\mathbf{Q}}}_{11}(r_n) + (\overline{\overline{\mathbf{I}}} + \overline{\overline{\mathbf{Q}}}_{12}(r_n))\left[\overline{\overline{\mathbf{I}}} - \overline{\overline{\mathbf{T}}}(r_{n-1})\overline{\overline{\mathbf{Q}}}_{22}(r_n)\right]^{-1}\overline{\overline{\mathbf{T}}}(r_{n-1})\left[\overline{\overline{\mathbf{I}}} + \overline{\overline{\mathbf{Q}}}_{21}(r_n)\right] \tag{46}$$

From this equation, It can be seen that if the T-matrix $\mathbf{T}(r_{n-1})$ of the sphere with $(n-1)$ layers is known, then the T-matrix $\mathbf{T}(r_n)$ of the sphere of nth spherical layers can be modified on the basis of $\mathbf{T}(r_{n-1})$, and the correction terms mainly depend on the optical properties of the nth spherical layer (through the matrix Q_{ij} (i, j = 1,2)).

2.4. Iterative Acceleration Based on the Lorenz–Mie Theory

According to Equation (46), during the implementation of the invariant embedding T-matrix method, the non-spherical particles are needed to be regarded as an inhomogeneous sphere and divided into a series of spherical shells. In this process, the optical matrices of spherical shells (including **U**, **Q** and $\boldsymbol{Q}_{ij}$ (i, j = 1, 2)) should be calculated first, then, the T-matrix of the sphere with n layers can be calculated based on the T-matrix of the smaller one with n − 1 layers.

In the calculation of the T-matrix, if we do the iteration directly from the origin of the sphere (r = 0) to the circumscribed spherical shell (r = R), the computational amount will be very large, which will limit the calculation efficiency of the model. In order to solve this problem, the scattering calculation region of particles is divided into two parts (as shown in Figure 2): one is the spherical core region with a radius of R_0 (R_0 is the radius of the particle's inscribed sphere), the other is the spherical mantle region in $R_0 < r < R$ (the region between the inscribed and circumscribed sphere). The spherical core region is a homogeneous sphere, and its T-matrix can be calculated by the Lorenz–Mie theory. While in the spherical mantle region, the invariant embedding technique is applied to solve the T-matrix, and its initial iteration value is set as the T-matrix of the spherical core. In this way, the unnecessary iteration process can be reduced, and the computational efficiency can be improved as well.

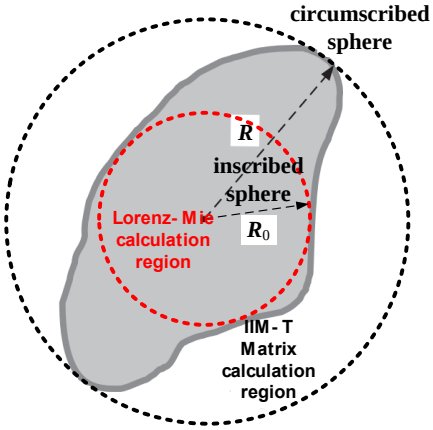

Figure 2. A schematic diagram of the division of the calculation region of the non-spherical scatterer. In this figure, R_0 is the radius of the inscribed sphere, while R is the radius of the circumscribed sphere.

A specific interface is needed to convert the Mie coefficients into the T-matrix of the inscribed sphere. For spheres, its T-matrix is a diagonal matrix, which satisfies $\mathbf{T}^{ij}_{mnm'n'} = \delta_{m,m'}\delta_{n,n'} \cdot \mathbf{T}^{ij}_{mnm'n'}$, so the relationship between the $\mathbf{T}$ and Mie coefficients (i.e., a_n and b_n) can be expressed as:

$$\mathbf{T}^{11}_{mnm'n'} = -\delta_{m,m'}\delta_{n,n'} \cdot b_n \tag{47}$$

$$\mathbf{T}^{22}_{mnm'n'} = -\delta_{m,m'}\delta_{n,n'} \cdot a_n \tag{48}$$

in which, a_n and b_n can be calculated by:

$$a_n = \frac{m\psi_n(mx)\psi'_n(x) - \psi_n(x)\psi'_n(mx)}{m\xi_n(mx)\psi'_n(x) - \xi_n(x)\psi'_n(mx)} \tag{49}$$

$$b_n = \frac{m\psi_n(x)\psi'_n(mx) - \psi_n(mx)\psi'_n(x)}{m\xi_n(x)\psi'_n(mx) - \xi_n(mx)\psi'_n(x)} \tag{50}$$

where, x is the size parameter of the inscribed sphere, and $\psi_n(x)$ and $\xi_n(x)$ are the Riccati–Bessel functions.

Based on the principle introduced above, the implementation of the IIM T-Matrix method can be concluded as follows:

Step 1: Determine the inscribed and circumscribed sphere of the non-spherical particle, and calculate the T-matrix of the inscribed sphere with the Lorenz–Mie Theory by using Equations (47)–(50).

Step 2: Taking the T-matrix of the inscribed sphere as the initial value, then the T-matrix of non-spherical particles is updated layer by layer by using Equation (46). The computational flowchart of the optical matrix of the spherical shell is presented in Figure 3. Firstly, the U-matrix is calculated by Equation (24), and then, the Q-matrix is directly calculated from the U-matrix by Equation (33). After the Q-matrix is obtained, $\mathbf{Q}_{11}$, $\mathbf{Q}_{12}$, $\mathbf{Q}_{21}$, and $\mathbf{Q}_{22}$ can be computed by Equations (37), (38), (42) and (43).

Step 3: After the T-matrix of the non-spherical particles is obtained, then the cross-sections can be directly linked to the elements of the T-matrix, and the phase matrix elements can also be obtained by combining the generalized spherical functions and T-matrix elements, readers can see Reference [16] for the details.

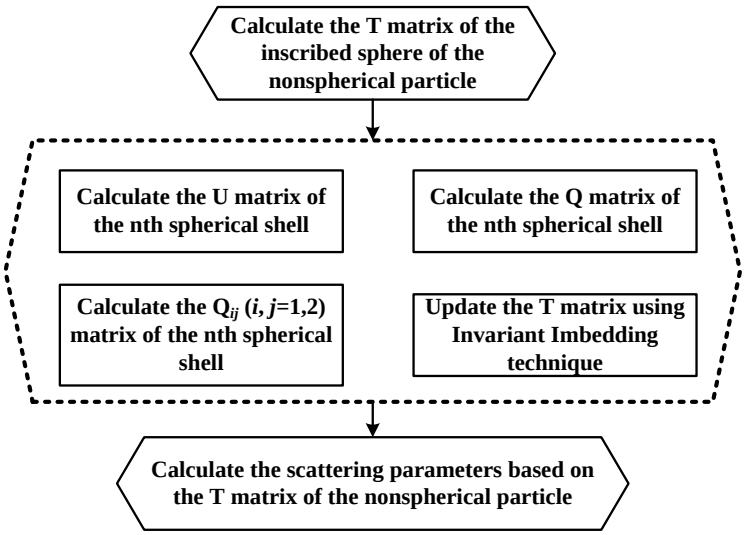

Figure 3. A schematic diagram of the implementation of our invariant imbedded (IIM) T-Matrix code.

3. Model Validation and Results Analysis

The invariant imbedded T-matrix model is implemented in Fortran95, and to improve the modeling efficiency, the model is further parallelized by the OpenMP technique (OpenMP is a multi-threading implementation technique that allows the compiler to generate code for task and data parallelism). To validate the simulation accuracy of this model, the scattering parameters calculated by the IIM T-Matrix method are compared with those calculated by EBCM and DDASCAT (which have been well tested and are usually taken as a benchmark). The non-spherical particles simulated in this paper include spheroid with different sizes, cylinder, spheroid with a spherical core (inhomogeneous particle), and hexagonal prism (particles with non-rotationally geometry).

3.1. Small Spheroidal Particle Case

In this simulation, the incident light wavelength is taken as $\lambda = 0.5$ μm (the typical wavelength in the visible band), the refractive index is set as $m = 1.60 - 0.008i$ (the typical value of mineral dust aerosol), the half-length of the horizontal and rotational axis are taken as $a = 1.0$ μm and $b = 0.5$ μm, and the scattering phase matrix of the spheroid is simulated by the IIM T-Matrix method and the EBCM T-Matrix method, respectively. The results are shown in Figure 4.

As shown in the figure, the results obtained by the two models are in good agreement, which verifies the simulation accuracy of the IIM T-Matrix model for the non-spherical particles with small size. For the phase function F_{11}, the relative errors are less than 5% in forward scattering directions. Though the calculation errors are relatively large near 180°, they are still smaller than 12%. For F_{12}/F_{11}, the calculation errors of the IIM T-Matrix model are all within 0.1, while the simulation errors of F_{34}/F_{11} and F_{44}/F_{11} are less than 0.1 in most scattering angles. From the spatial distribution of simulation errors, it can be found that the simulation accuracy of the IIM T-Matrix model in the forward scattering direction is obviously higher than that in large scattering angles. The reason is that, in the IIM T-Matrix model, the particle is discretized in a spherical coordinate system, and similar to PSTD and MRTD, there are also stepped approximation errors in shape construction. Further, because the scattering phase matrix is more sensitive to the particle's shape in backscattering directions, larger simulation errors will be caused in large scattering angles correspondingly.

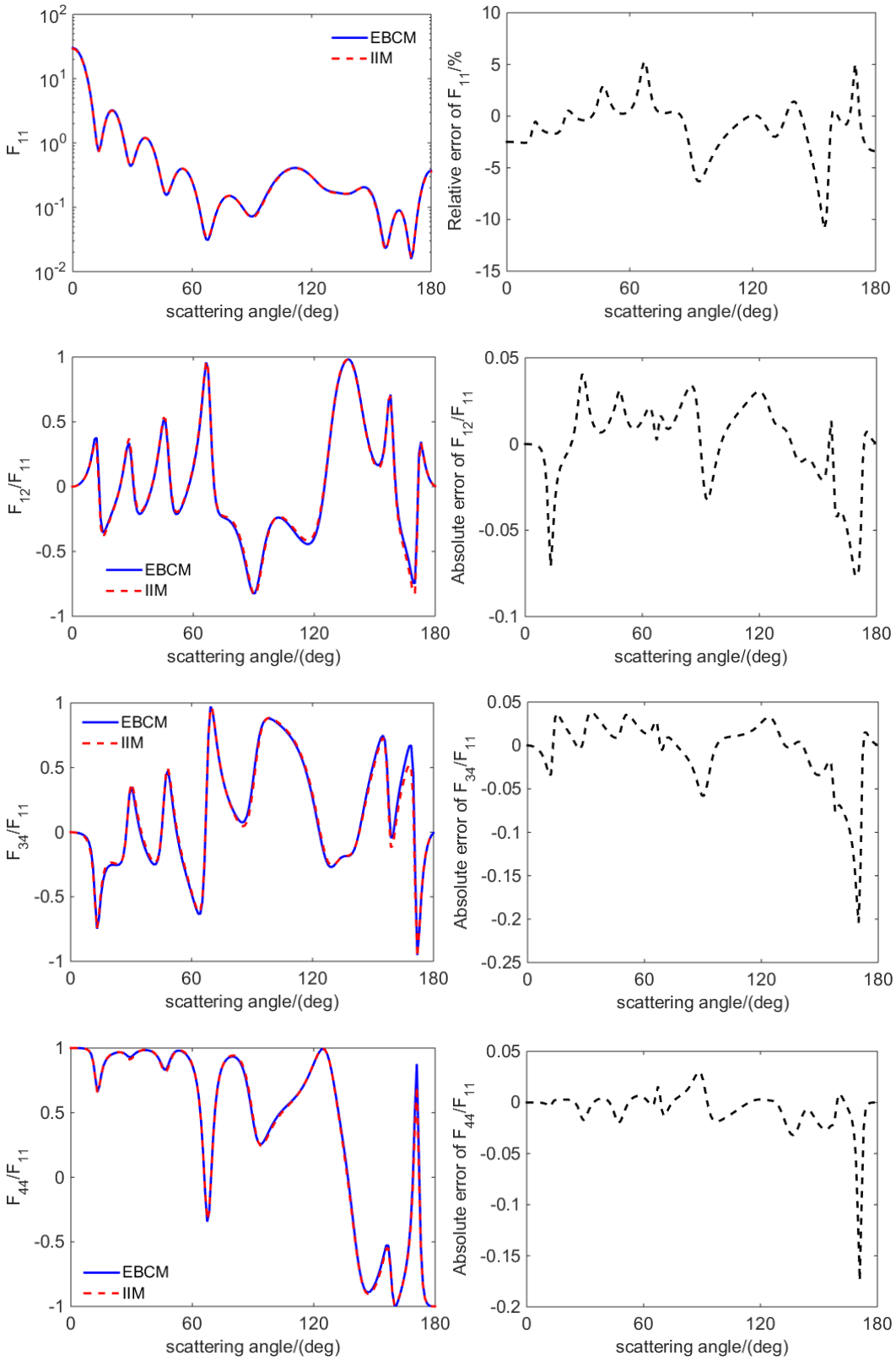

Figure 4. The scattering phase matrix obtained by the IIM and Extended Boundary Condition Method (EBCM) T-Matrix methods for small spheroid particles. The simulation errors of F_{11} are denoted by relative errors. For F_{12}, F_{34}, and F_{44}, they are firstly normalized by F_{11}, and their simulation errors are evaluated by the absolute errors.

To further validate the simulation accuracy of the IIM T-Matrix method, the integral scattering parameters (including extinction cross-section C_{ext}, absorption cross-section C_{abs}, scattering cross-section C_{sca}, and single scattering albedo ω) are also compared with those obtained by EBCM, the results are shown in Table 1. It can be found that the relative simulation errors of the integral scattering parameters are generally smaller than 1%, indicating that the integral scattering parameters can be calculated by the IIM T-Matrix method with a high accuracy.

Table 1. The integral scattering parameters calculated by the IIM and EBCM T-Matrix methods for the small spheroidal particle.

Model Type	$C_{ext}/\mu m^2$	$C_{abs}/\mu m^2$	$C_{sca}/\mu m^2$	ω
EBCM	4.889	0.0953	4.793	0.98036
IIM T-Matrix	4.872	0.0957	4.776	0.98029
Difference/%	0.3489	−0.4179	0.3559	0.00698

3.2. Large Spheroidal Particle Case

To validate the calculation precision of the IIM T-Matrix method for particles with large sizes, light scattering by a large spheroid particle is simulated by the IIM T-Matrix method and EBCM, respectively, and the result is shown in Figure 5. In this simulation, the light wavelength is set as $\lambda = 0.6$ μm, the refractive index of the particle is taken to be $m = 1.60 - 0.0008i$, and the length of the horizontal and rotational axes are set as $a = 4.5$ μm and $b = 6.0$ μm, respectively. The region between the inscribed and circumscribed spheres is divided into 50 layers along the radial direction.

From the figures, it can be found that the scattering phase matrix obtained by the IIM T-Matrix model shows a high consistency with that obtained by EBCM, indicating that the IIM T-Matrix method can simulate the large non-spherical particle effectively. For F_{11}, the relative simulation errors are all less than 10% in the scattering angles ranging from 0° to 120°. Though the simulation errors are slightly larger in the scattering angles in large scattering angles, its maximum error is smaller than 15%. For F_{12}/F_{11} and F_{44}/F_{11}, the calculation errors of the IIM-T-matrix model are less than 0.05 in most scattering directions, especially in scattering angles ranging from 0° to 60°, the modeling accuracy is much higher than other scattering directions. The simulation accuracy of F_{34}/F_{11} is slightly lower than that of F_{12}/F_{11} and F_{44}/F_{11}, but their simulation errors are still less than 0.1 at most scattering angles. Similar to the small spheroidal particle, the simulation accuracy is lower in the large scattering angles, while in the forward scattering directions, the simulation errors are much smaller.

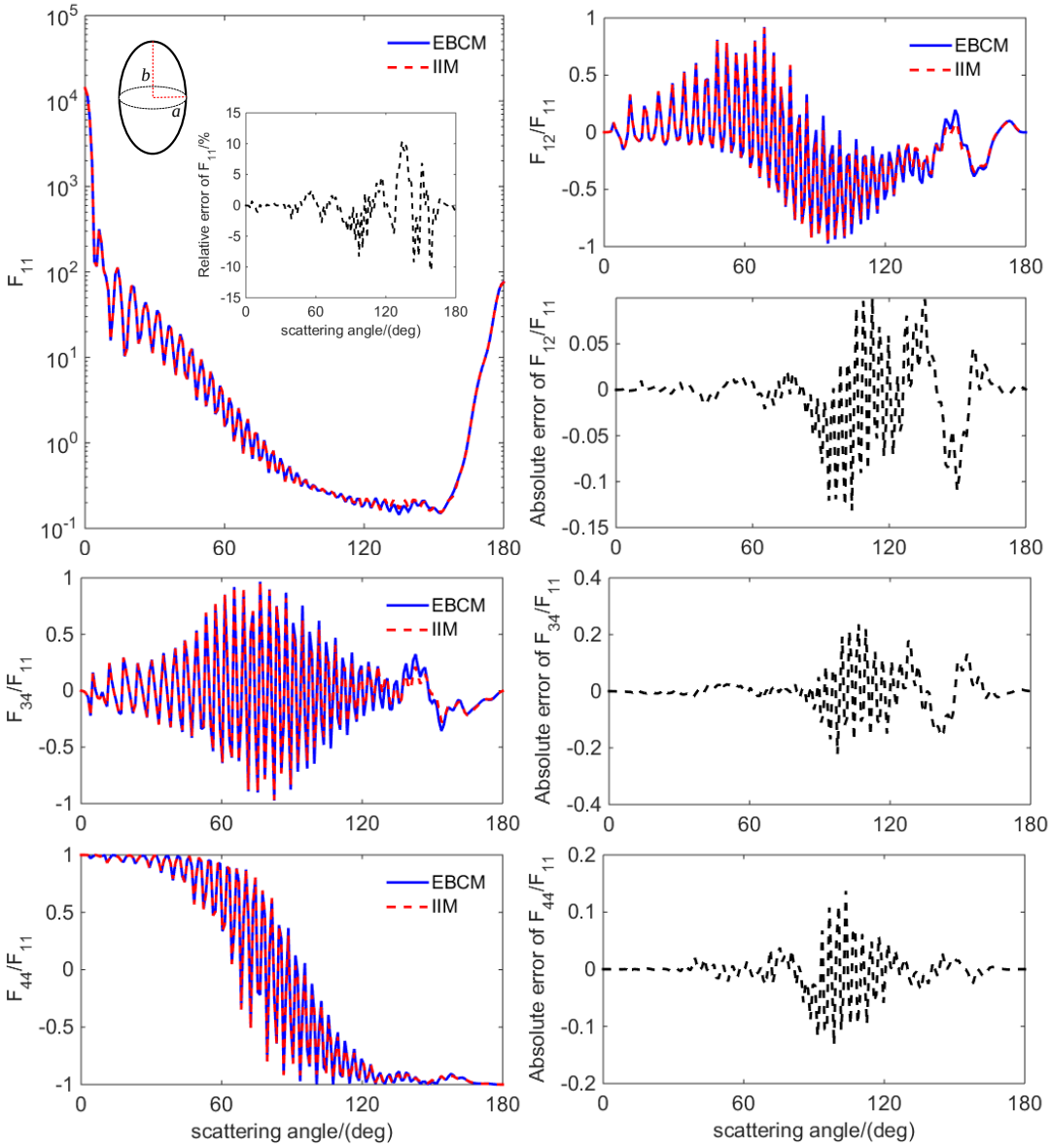

Figure 5. The scattering phase matrix obtained by the IIM and EBCM T-Matrix methods for the large spheroid particle. The simulation errors of F_{11} are denoted by relative errors. For F_{12}, F_{34}, and F_{44}, they are firstly normalized by F_{11}, and their simulation errors are evaluated by the absolute errors.

Similar to Section 3.1, the integral scattering parameters of the large spheroid of our model are also compared with those of EBCM, the results are presented in Table 2. As can be seen, a good consistency is achieved between the results obtained by different models. The relative differences of these parameters are all less than 0.5%, which indicates that the IIM T-Matrix method can simulate the scattering process of large particles accurately.

Table 2. The integral scattering parameters calculated by the IIM and EBCM T-Matrix methods for the large spheroidal particle.

Model Type	$C_{ext}/\mu m^2$	$C_{abs}/\mu m^2$	$C_{sca}/\mu m^2$	ω
EBCM	165.918	13.18	152.739	0.9205
IIM T-Matrix	165.687	13.134	152.553	0.9207
Difference/%	0.1394	0.3502	0.1219	−0.0175

3.3. Cylindrical Particle Case

The modeling capability of the IIM T-Matrix model is investigated for cylindrical particles. In this test, the light wavelength is taken as 0.5 μm, the refractive index of the particle is set as $m = 1.60 - 0.0008i$, and the diameter (D) and length (L) of the cylinder are set as 2 μm. The scattering phase matrices are calculated by the EBCM and IIM T-Matrix methods, and the results are shown in Figure 6.

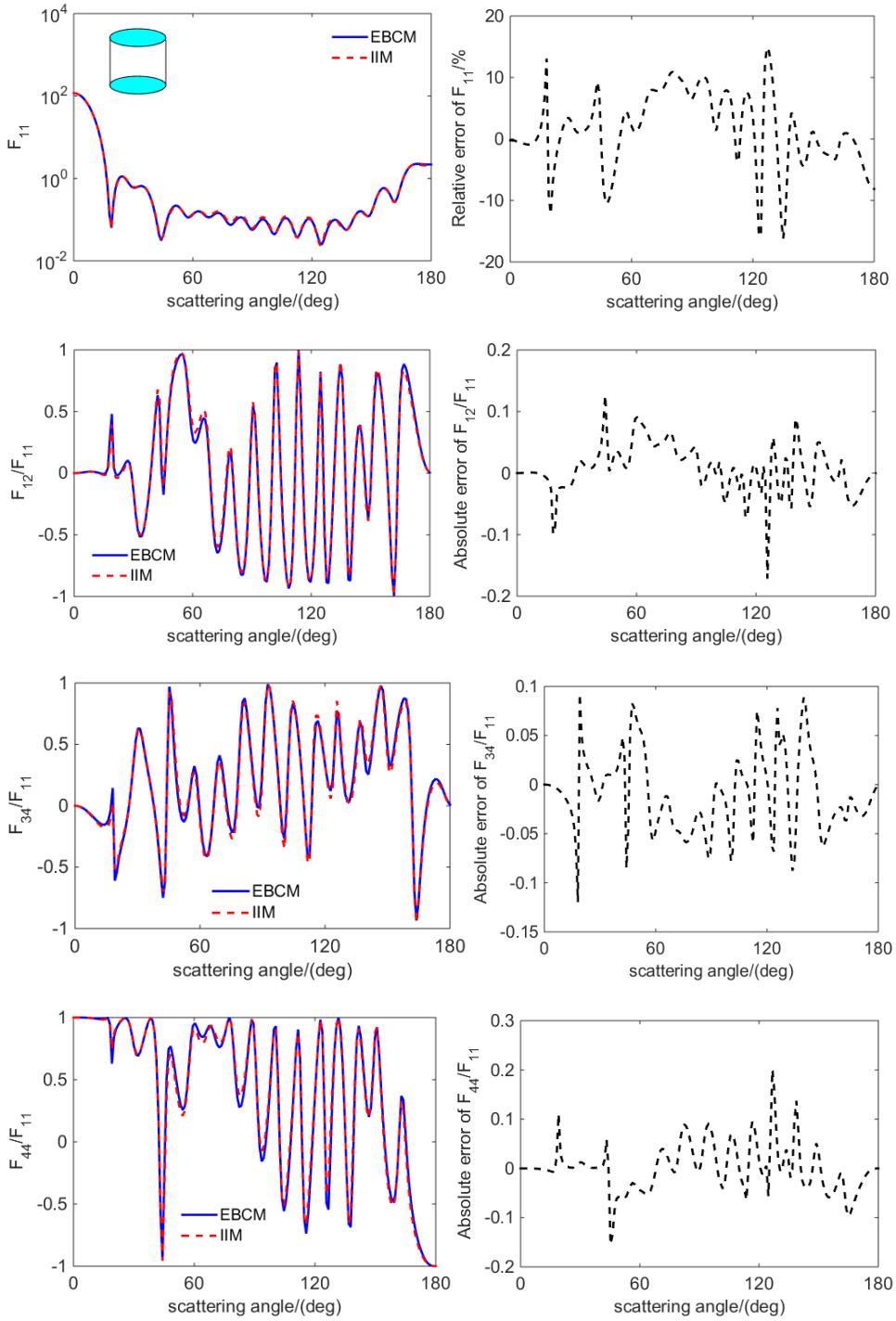

Figure 6. The scattering phase matrix obtained by the IIM and EBCM T-Matrix methods for cylindrical particles. The simulation errors of F_{11} are denoted by relative errors. For F_{12}, F_{34}, and F_{44}, they are firstly normalized by F_{11}, and their simulation errors are evaluated by the absolute errors.

It can be seen that the results calculated by the IIM T-Matrix model show a good agreement with those of EBCM, indicating that the IIM T-Matrix method can simulate the light scattering process of a cylinder with a high accuracy. For F_{11}, its relative errors are less than 10% in most scattering directions, and for F_{12}/F_{11}, F_{34}/F_{11}, and F_{44}/F_{11}, their absolute errors are generally smaller than 0.1. Similar to the results of spheroidal particles, the spatial distribution of simulation errors is similar to the variation pattern of the phase matrix elements; namely, in the scattering directions where the curves of the phase matrix elements change dramatically, their simulation errors will increase as well.

The integral scattering parameters of different models are also calculated, as shown in Table 3. It can be found that the results of the IIM T-Matrix method show a good agreement with those of EBCM, which validates the modeling accuracy of the IIM T-Matrix method.

Table 3. The integral scattering parameters calculated by the IIM and EBCM T-Matrix methods for the cylindrical particle.

Model Type	$C_{ext}/\mu m^2$	$C_{abs}/\mu m^2$	$C_{sca}/\mu m^2$	ω
EBCM	11.4129	0.2791	11.1338	0.9755
IIM T-Matrix	11.3102	0.2735	11.0367	0.9758
Difference/%	0.9080	2.0475	0.8798	−0.0279

3.4. Inhomogeneous Particle Case

To verify the modeling capability of the IIM T-Matrix method for particles with inhomogeneous compositions, the results obtained by the IIM T-matrix model are compared with the DDASCAT for a spheroid with a spherical core. In this case, the wavelength of incident light is taken as 0.5 μm, the horizontal and rotational axis of the outer spheroid are set as a = 1.0 μm and b = 1.5 μm respectively, and its complex refractive index is set to be $m_1 = 1.44 - 0.000i$. The inner part is a spherical core with a radius of 1.0 μm, its refractive index is taken as $m_2 = 1.20 - 0.000i$. The region between the inscribed and circumscribed spheres is divided into 30 layers along the radial direction. The simulation results are shown in Figure 7.

As can be seen from the figure, the IIM-T-matrix model achieves high calculation accuracy, and the curves of the scattering phase matrix are almost coincided with those of DDASCAT. For F_{11}, the relative simulation errors are all less than 10% in scattering angles ranging from 0° to 30°. With the increase of scattering angle, its simulation accuracy decreases, but the relative errors are within 26%. The spatial distributions of the simulation errors of F_{12}/F_{11}, F_{34}/F_{11}, and F_{44}/F_{11} are similar to F_{11}. In the forward scattering direction, their simulation accuracy is higher and the absolute simulation errors tend to be 0, while as the scattering angle becomes larger, their simulation accuracy is slightly reduced, but it should be noted that their absolute simulation errors are still within 0.1 in most scattering directions. From the discussion, it can be found that the IIM T-Matrix method can simulate the light scattering by inhomogeneous particles with a high accuracy.

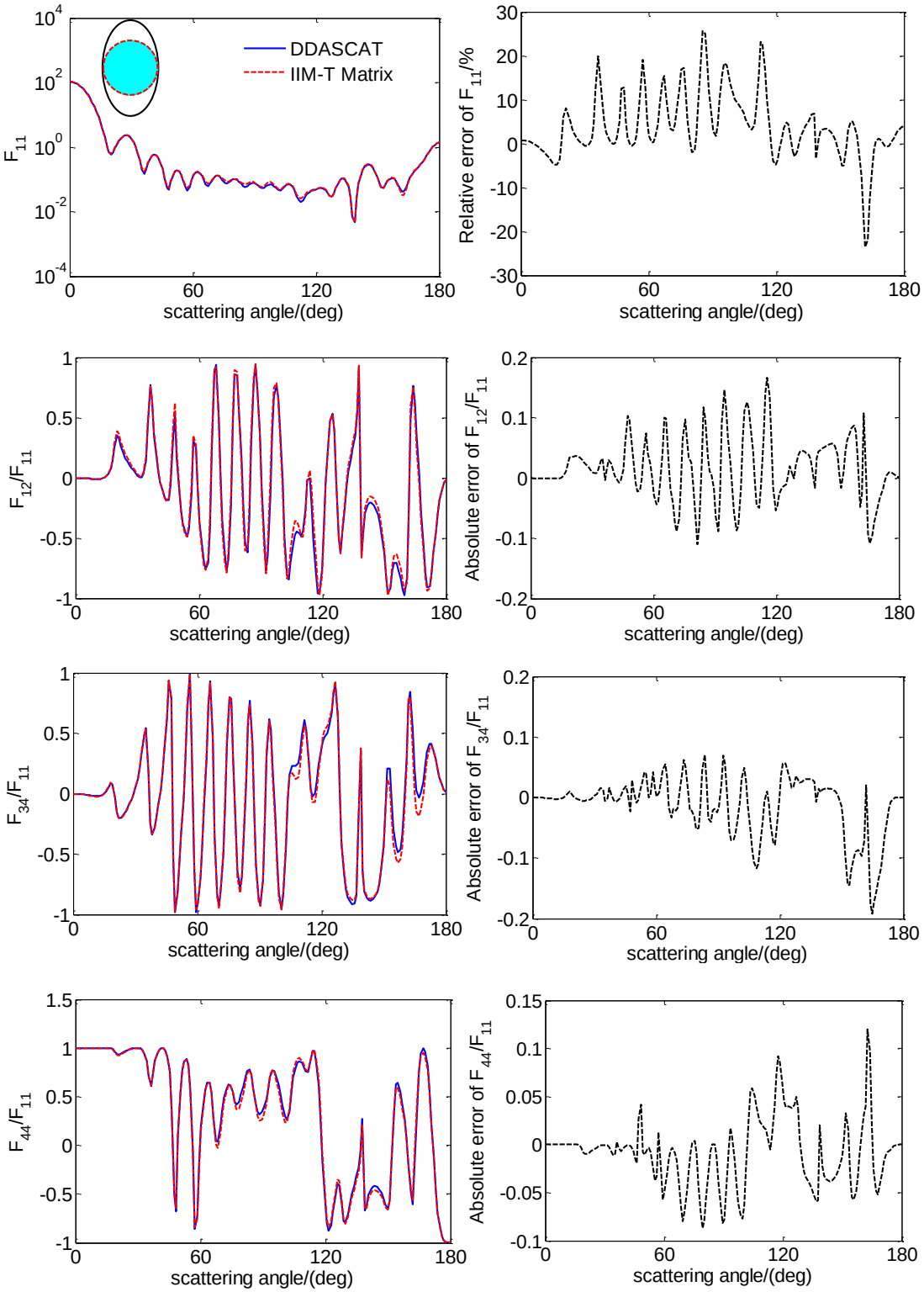

Figure 7. The scattering phase matrix obtained by the IIM T-Matrix method and DDASCAT for the spheroidal particle with a spherical core. The simulation errors of F_{11} are denoted by relative errors. For F_{12}, F_{34}, and F_{44}, they are firstly normalized by F_{11}, and their simulation errors are evaluated by the absolute errors.

3.5. Hexagonal Prism Case

To validate the simulation accuracy of the IIM T-Matrix method for non-rotational symmetric particles (which cannot be effectively simulated by the EBCM T-Matrix method), the results of the IIM T-Matrix method are further compared with that of the MRTD model developed by our team [27,41].

The MRTD scattering model is established based on the Multi-Resolution Time Domain technique. By using this model, light scattering by arbitrarily shaped particles or ice crystals can be effectively simulated. In this model, the plane wave is introduced into the computational space by the TF/SF (Total Field/Scattering Field) technique, the Convolution Perfectly Matched Layer (CPML) is applied to truncate the computational domain, and the volume integral method is employed to transform the near electric field to the far field.

In this simulation, the light wavelength and refractive index are set as $\lambda = 0.5$ μm and $m = 1.20 - 0.0008i$, and the length and bottom edge length of hexagonal prism are set as $L = 2.0$ μm and $a = 1.0$ μm, respectively. The results are shown in Figure 8.

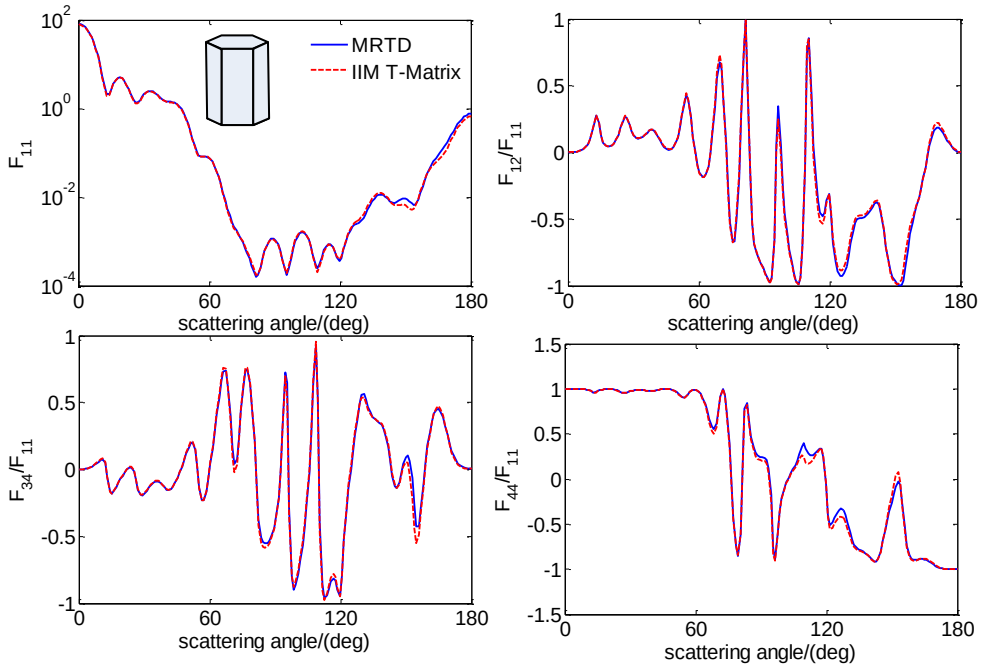

Figure 8. The scattering phase matrix obtained by the IIM T-Matrix method and Multi-Resolution Time Domain (MRTD) for hexagonal prism.

As can be seen, a high agreement is achieved between the results of the T-matrix method and those of the MRTD model, which indicates that both MRTD and IIM-T-matrix models can effectively simulate the scattering characteristics of a hexagonal prism. Similar to the conclusion drawn above, the consistency of the two models in forward scattering directions is higher than those at large scattering angles, where for the scattering phase functions F_{11}, the relative simulation errors tend to be zero in scattering angles smaller than 30°, while in scattering directions near 170°, the simulation accuracy is relatively lower, and the maximum simulation errors can reach 36.7%.

4. Analysis of Modeling Efficiency

To further validate the effectiveness of the iterative acceleration scheme based on the Lorenz–Mie theory, the computational efficiency of the improved model is investigated as well. In those simulations, the light wavelength is set as 0.5 μm, and the scatterers are set as spheroidal particles with different shapes. All the scattering processes are simulated on the same computer (32 bit 3.1 GHz), and the computational time of the traditional and improved IIM T-Matrix code is presented in Table 4.

Table 4. The computational time needed for the IIM T-Matrix model with and without the Lorenz–Mie theory.

(a, b)	Number of Threads	Computational Time T_0 of the Model without Lorenz–Mie Theory/s	Computational Time T_1 of the Model with Lorenz–Mie Theory/s	$(T_0 - T_1)/T_0 \times 100\%$
(1.5, 2.0)	4	4463	1111	75.10643
(1.0, 2.0)	4	4438	2232	49.70708
(0.7, 2.0)	4	4485	2879	35.80825

As can been seen, after being improved by the iterative acceleration scheme, the computational efficiency of the IIM T-Matrix method is improved notably, where for the particle with (a, b) = (1.5, 2.0), the computational time is cut down by 75%. With the increase of the aspect ratio (a/b), the improvement of the computational efficiency is much more remarkable.

5. Conclusions

The T-matrix is a complete scattering information set that only depends on the particle size, refractive index, and shape; therefore, once the T-matrix is obtained, the scattering properties of the particles with arbitrary orientations can be calculated analytically, which is a tremendous advantage over DDA, FDTD, and other scattering models. In this paper, a T-matrix scattering model was developed by combining the invariant imbedding iterative technique and the Lorenz–Mie theory. Compared with the T-Matrix model developed by Mishchenko, it can be applied to the light scattering simulation of particles with arbitrary shape and inhomogeneous compositions. In this paper, the basic principle of the IIM T-Matrix method was firstly derived, and then, an iterative acceleration scheme was proposed based on the Lorenz–Mie theory and the invariant imbedding technique. To improve the computational efficiency, the model was further parallelized by the OpenMP technique. To validate the calculation accuracy of the model, the scattering phase matrix computed by the IIM T-Matrix method was compared with that of EBCM, DDASCAT, and MRTD. The results show that good agreements were achieved between the results of the IIM T-Matrix method and those well-tested scattering models, indicating that the IIM T-Matrix method can accurately simulate the scattering properties of non-spherical particles with different shapes and inhomogeneous compositions. After being improved by the iterative acceleration scheme based on the Lorenz–Mie theory, the computational efficiency of the IIM T-Matrix method was improved notably. Owning to its excellent performance, the IIM T-Matrix model might become a powerful tool for the light scattering simulation of non-spherical particles in the atmospheric radiation field.

Author Contributions: Conceptualization, S.H. and L.L.; methodology, S.H.; software, S.H.; validation, S.H., L.L. and T.G.; writing—original draft preparation, S.H.; writing—review and editing, Q.Z.; project administration, L.L.; funding acquisition, L.L.

Funding: This research was funded by the National Science Foundation of China, grant number 41575025, 41575024.

Acknowledgments: Thanks for the T-matrix code provided by M. I. Mishchenko. (http://www.giss.nasa.gov/staff/mmishchenko/t_matrix.html).

Conflicts of Interest: The authors declare no conflict of interest.

Appendix A

Vector spherical harmonic functions in the IIM T-Matrix method are obtained by solving the vector Helmholtz equation by the separation of variables method, and their expressions can be written as follows [42]:

$$Rg\mathbf{M}_{mn}(kr,\theta,\varphi) = \left(\frac{2n+1}{4\pi n(n+1)}\right)^{1/2}(-1)^m \exp(\mathrm{i}m\varphi)\left(\hat{\boldsymbol{\theta}} i\pi_{mn}(\theta) - \hat{\boldsymbol{\varphi}}\tau_{mn}(\theta)\right)J_n(kr) \quad \text{(A1)}$$

$$Rg\mathbf{N}_{mn}(kr,\theta,\varphi) = \left(\frac{2n+1}{4\pi n(n+1)}\right)^{1/2}(-1)^m \exp(\mathrm{i}m\varphi) \times\left[\frac{n(n+1)}{kr}J_n(kr)\cdot d^n_{0m}\hat{\mathbf{r}} + \frac{1}{kr}\frac{d}{d(kr)}(krJ_n(kr))\left(\hat{\boldsymbol{\theta}}\tau_{mn}(\theta) + \hat{\boldsymbol{\varphi}}i\pi_{mn}(\theta)\right)\right] \tag{A2}$$

$$\mathbf{M}_{mn}(kr,\theta,\varphi) = \left(\frac{2n+1}{4\pi n(n+1)}\right)^{1/2}(-1)^m \exp(\mathrm{i}m\varphi)\left(\hat{\boldsymbol{\theta}}i\pi_{mn}(\theta) - \hat{\boldsymbol{\varphi}}\tau_{mn}(\theta)\right)H^{(1)}_n(kr) \tag{A3}$$

$$\mathbf{N}_{mn}(kr,\theta,\varphi) = \left(\frac{2n+1}{4\pi n(n+1)}\right)^{1/2}(-1)^m \exp(\mathrm{i}m\varphi) \times\left[\frac{n(n+1)}{kr}H^{(1)}_n(kr)\cdot d^n_{0m}\hat{\mathbf{r}} + \frac{1}{kr}\frac{d}{d(kr)}\left(krH^{(1)}_n(kr)\right)\left(\hat{\boldsymbol{\theta}}\tau_{mn}(\theta) + \hat{\boldsymbol{\varphi}}i\pi_{mn}(\theta)\right)\right] \tag{A4}$$

From the equations above, it can be found that the vector spherical harmonic functions can be divided into 3 parts: the azimuth angle component, the radial component, and the scattering angle component. The azimuth angle component is denoted as $\exp(\mathrm{i}m\varphi)$, the radial component is a combination of the spherical Bessel functions, where, in $Rg\mathbf{M}_{mn}$ and $Rg\mathbf{N}_{mn}$, the first kind of Bessel function $J_n(kr)$ is used, while in $\mathbf{M}_{mn}$ and $\mathbf{N}_{mn}$, the Hankel function of the first kind is applied. The scattering angle component is a vector, which is constructed by the angular functions, i.e., $\pi_{mn}(\theta)$ and $\tau_{mn}(\theta)$, and the Wigner-d function $d^n_{0m}(\theta)$.

References

1. Liou, K.-N.; Yang, P. *Light Scattering by Ice Crystals*; Cambridge University Press: Cambridge, UK, 2016.
2. Liou, K.N. *An Introduction to Atmospheric Radiation*; Academic Press: San Diego, CA, USA, 2003.
3. Zhang, F.; Wu, K.; Li, J.; Yang, Q.; Zhao, J.-Q.; Li, J. Analytical infrared delta-four-stream adding method from invariance principle. *J. Atmos. Sci.* **2016**, *73*, 4171–4188. [CrossRef]
4. Zhang, F.; Li, J. Doubling–adding method for delta-four-stream spherical harmonic expansion approximation in radiative transfer parameterization. *J. Atmos. Sci.* **2013**, *70*, 3084–3101. [CrossRef]
5. Zhao, J.-Q.; Hu, Y.-Q. Bridging technique for calculating the extinction efficiency of arbitrary shaped particles. *Appl. Opt.* **2003**, *42*, 4937–4945. [CrossRef]
6. Zhao, J.-Q.; Shi, G.; Chen, H.; Cheng, G. Approximation of scattering phase function of particles. *Adv. Atmos. Sci.* **2006**, *23*, 802–808. [CrossRef]
7. Zhao, J.-Q. Simple technique to evaluate effects of nonsphericity and orientation on particle size distribution retrieval. *Int. J. Phys. Sci.* **2011**, *6*, 7100–7105.
8. Curtis, D.B.; Meland, B.; Aycibin, M. A laboratory investigation of light scattering from representative components of mineral dust aerosol at a wavelength of 550 nm. *J. Geophys. Res.* **2008**, *113*, D08210. [CrossRef]
9. Dubovik, O.; Sinyuk, A.; Lapyonok, T.; Holben, B.N.; Mishchenko, M.; Yang, P.; Eck, T.F.; Volten, H.; Munoz, O.; Veihelmann, B.; et al. Application of spheroid models to account for aerosol particle nonsphericity in remote sensing of desert dust. *J. Geophys. Res.* **2006**, *111*, D11208. [CrossRef]
10. Deuzé, J.L.; Goloub, P.; Herman, M.; Marchand, A.; Perry, G. Estimate of the aerosol properties over the ocean with polder. *J. Geophys. Res.* **2000**, *105*, 15329–15346. [CrossRef]
11. Deuzé, J.L.; Bréon, F.M.; Devaux, C.; Goloub, P.; Herman, M.; Lafrance, B.; Maignan, F.; Marchand, A.; Nadal, F.; Perry, G.; et al. Remote sensing of aerosols over land surfaces from polder-adeos-1 polarized measurements. *J. Geophys. Res.* **2001**, *106*, 4913–4926. [CrossRef]
12. Sun, W.; Videen, G.; Fu, Q.; Hu, Y. Scattered-field fdtd and pstd algorithms with cpml absorbing boundary conditions for light scattering by aerosols. *J. Quant. Spectrosc. Radiat. Transf.* **2013**, *131*, 166–174. [CrossRef]
13. Mishchenko, M.I.; Travis Larry, D. Satellite retrieval of aerosol properties over the ocean using polarization as well as intensity of reflected sunlight. *J. Geophys. Res.* **1997**, *102*, 16989–17014. [CrossRef]
14. Hu, S.; Gao, T.; Li, H.; Liu, L.; Liu, X.-C.; Zhang, T.; Cheng, T.-J.; Li, W.-T.; Dai, Z.-H.; Su, X.-J. Effect of atmospheric refraction on radiative transfer in visible and near-infrared band: Model development, validation, and applications. *J. Geophys. Res. Atmos.* **2016**, *121*, 2349–2368. [CrossRef]
15. Mishchenko, M.I.; Hovenier, J.W.; Travis, L.D. *Light Scattering by Nonspherical Particles, Thoery, Measurements, and Application*; Academic Press: New York, NY, USA, 2000.

16. Mishchenko, M.I.; Travis, L.D.; Lacis, A.A. *Scattering, Absorption, and Emission of Light by Small Particles*; Cambridge University Press: New York, NY, USA, 2002.
17. Mishchenko, M.I.; Travis, L.D. T-martrix computations of light scattering by large spheriodal particles. *Opt. Commun.* **1994**, *109*, 16–21. [CrossRef]
18. Mishchenko, M.I.; Travis, L.D. Capabilities and limitations of a current fortran implementation of the t-martrix method for randomly oriented, rotationally symmetric scatterers. *J. Quant. Spectrosc. Radiat. Transf.* **1998**, *60*, 309–324. [CrossRef]
19. Draine, B.T.; Flatau, P.J. Discrete-dipole approximation for periodic targets: Theory and tests. *J. Opt. Soc. Am. A* **2008**, *25*, 2693–2703. [CrossRef] [PubMed]
20. Yurkin, M.A.; Hoekstra, A.G. The discrete-dipole-approximation code adda: Capabilities and known limitations. *J. Quant. Spectrosc. Radiat. Transf.* **2011**, *112*, 2234–2247. [CrossRef]
21. Yang, P.; Liou, K.N. Finite-difference time domain method for light scattering by small ice crystals in three-dimensional space. *J. Opt. Soc. Am. A* **1996**, *13*, 2073–2085. [CrossRef]
22. Sun, W.; Fu, Q. Finite-difference time-domain solution of light scattering by dielectric particles with large complex refractive indices. *Appl. Opt.* **2000**, *39*, 5569–5578. [CrossRef]
23. Liu, C.; Panetta, R.L.; Yang, P. Application of the pseudo-spectral time domain method to compute particle single-scattering properties for size parameters up to 200. *J. Quant. Spectrosc. Radiat. Transf.* **2012**, *113*, 1728–1740. [CrossRef]
24. Hu, S.; Gao, T.; Liu, L.; Li, H.; Chen, M.; Yang, B. Application of the weighted total field-scattering field technique to 3d-pstd light scattering model. *J. Quant. Spectrosc. Radiat. Transf.* **2018**, *209*, 58–72. [CrossRef]
25. Hu, S.; Gao, T.; Li, H.; Liu, L.; Chen, M.; Yang, B. Light-scattering model for aerosol particles with irregular shapes and inhomogeneous compositions using a parallelized pseudo-spectral time-domain technique. *Chin. Phys. B* **2018**, *27*, 054215. [CrossRef]
26. Hu, S.; Gao, T.; Li, H.; Yang, B.; Zhang, F.; Chen, M.; Liu, L. Light scattering computation model for nonspherical aerosol particles based on multi-resolution time-domain scheme: Model development and validation. *Opt. Express* **2017**, *25*, 1643–1686. [CrossRef] [PubMed]
27. Hu, S.; Gao, T.; Li, H.; Yang, B.; Jiang, Z.; Liu, L.; Chen, M. Application of convolution perfectly matched layer in mrtd scattering model for non-spherical aerosol particles and its performance analysis. *J. Quant. Spectrosc. Radiat. Transf.* **2017**, *200*, 1–11. [CrossRef]
28. Mishchenko, M.I. Calculation of the amplitude matrix for a nonspherical particle in a fixed orientation. *Appl. Opt.* **2000**, *39*, 1026–1031. [CrossRef] [PubMed]
29. Waterman, P.C. Matrix formulation of electromagnetic scattering. *Proc. IEEE* **1965**, *53*, 805–812. [CrossRef]
30. Waterman, P.C. Symmetry, unitarity, and geometry in electromagnetic scattering. *Phys. Rev. D* **1971**, *3*, 825–839. [CrossRef]
31. Bi, L.; Yang, P.; Kattawar, G.W.; Mishchenko, M.I. Efficient implementation of the invariant imbedding t-matrix method and the separation of variables method applied to large nonspherical inhomogeneous particles. *J. Quant. Spectrosc. Radiat. Transf.* **2013**, *116*, 169–183. [CrossRef]
32. Quirantes, A. A t-matrix method and computer code for randomly oriented, axially symmetric coated scatterers. *J. Quant. Spectrosc. Radiat. Transf.* **2005**, *92*, 373–381. [CrossRef]
33. Zubko, E.; Muinonen, K.; Muñoz, O.; Nousiainen, T.; Shkuratov, Y.; Sun, W.; Videen, G. Light scattering by feldspar particles: Comparison of model agglomerate debris particles with laboratory samples. *J. Quant. Spectrosc. Radiat. Transf.* **2013**, *131*, 175–187. [CrossRef]
34. Schulz, F.M.; Stamnes, K.; Stamnes, J.J. Scattering of electromagnetic waves by spheroidal particles: A novel approach exploiting the t matrix computed in spheroidal coordinates. *Appl. Opt.* **1998**, *37*, 7875–7896. [CrossRef]
35. Mackowski, D.W. Discrete dipole moment method for calculation of the t matrix for nonspherical particles. *J. Opt. Soc. Am. A* **2002**, *19*, 881–893. [CrossRef] [PubMed]
36. Loke, V.L.Y.; Nieminen, T.A.; Heckenberg, N.R.; Rubinsztein-Dunlop, H. T-matrix calculation via discrete dipole approximation, point matching and exploiting symmetry. *J. Quant. Spectrosc. Radiat. Transf.* **2009**, *110*, 1460–1471. [CrossRef]
37. Bi, L.; Yang, P.; Kattawar, G.W.; Mishchenko, M.I. A numerical combination of extended boundary condition method and invariant imbedding method applied to light scattering by large spheroids and cylinders. *J. Quant. Spectrosc. Radiat. Transf.* **2013**, *123*, 17–22. [CrossRef]

38. Bi, L.; Yang, P. Accurate simulation of the optical properties of atmospheric ice crystals with the invariant imbedding t-matrix method. *J. Quant. Spectrosc. Radiat. Transf.* **2014**, *138*, 17–35. [CrossRef]
39. Johnson, B.R. Invariant imbedding t matrix approach to electromagnetic scattering. *Appl. Opt.* **1988**, *27*, 4861–4873. [CrossRef] [PubMed]
40. Griffiths, D.J. *Introduction to Electrodynamics*, 3rd ed.; Prentice-Hall: Englewood, IL, USA, 1999.
41. Hu, S.; Gao, T.; Li, H.; Chen, M.; Zhang, F.; Yang, B. Simultaneously simulating the scattering properties of nonspherical aerosol particles with different sizes by the mrtd scattering model. *Opt. Express* **2017**, *25*, 17872–17891. [CrossRef]
42. Bohren, C.F.; Huffman, D.R. *Absorption and Scattering of Light by Small Particles*; John Wiley & Sons, Inc: New York, NY, USA, 1983.